1 Episodic subduction patches in the western North Pacific identified from BGC-Argo
2 float Data

3 Shuangling Chen[1], Mark L. Wells[2,1], Rui Xin Huang[3], Huijie Xue[2], Jingyuan Xi[1], Fei
4 Chai[1,2*]

5 [1] State Key Laboratory of Satellite Ocean Environment Dynamics, Second Institute of
6 Oceanography, Ministry of Natural Resources, Hangzhou, China

7 [2] School of Marine Sciences, University of Maine, Orono, ME, USA

8 [3] Woods Hole Oceanographic Institution, Woods Hole, MA, USA

9 [*]Corresponding author: Fei Chai (fchai@sio.org.cn)

10 **Abstract**

11 Subduction associated with mesoscale eddies is an important but difficult to observe
12 process that can efficiently export carbon and oxygen to the mesopelagic zone (100-
13 1000db). Using a novel BGC-Argo dataset covering the western North Pacific (20-
14 50°N, 120-180°E), we identified imprints of episodic subduction using anomalies in
15 dissolved oxygen and spicity, a water mass marker. These subduction patches were
16 present in 4.0% (288) of the total profiles (7,120) between 2008 and 2019, situated
17 mainly in the Kuroshio Extension region between March and August (70.6%). Roughly
18 31% and 42% of the subduction patches were identified below the annual permanent
19 pycnocline depth (300m *vs.* 450 m) in the subpolar and subtropical regions. ~~Unlike eddy~~
20 ~~subduction processes observed at higher latitudes, roughly~~ Around half (52%) of these
21 episodic events injected ~~carbon and~~ oxygen-enriched waters below the maximum
22 annual permanent thermocline depth (450 db), with >20% occurring deeper than 600
23 db. ~~Export rates~~Oxygen inventory within these subductions ~~are~~ is estimated to be on
24 the order of ~~85-159~~ ~~mg C m^{-2} day^{-1}~~ ~~and 175 to 417~~ 64 to 152 mg O_2 m^{-2} ~~day^{-1}~~. These
25 mesoscale events would markedly increase oxygen ventilation as well as carbon
26 removal ~~above that due to biological gravitational settling as well as oxygen ventilation~~
27 in the region, both helping to support the nutritional and metabolic demands of
28 mesopelagic organisms. Climate-driven patterns of increasing eddy kinetic energies in
29 this region imply that the magnitude of these processes will grow in the future, meaning
30 that these unexpectedly effective small-scale subduction processes need to be better
31 constrained in global climate and biogeochemical models.

32 **Keywords:** dissolved oxygen; spicity; BGC-Argo; subduction; North Pacific

33 **1. Introduction**

34 Ocean subduction is the process of transporting water from the wind-mixed surface
35 layer into or below the permanent thermocline, resulting in the efficient injection of
36 heat, carbon and oxygen to the ocean interior (Fig. 1). Subduction therefore plays an
37 important role in regulating global climate and carbon cycles (Sabine et al., 2004; Qu
38 ~~and~~ & Chen, 2009; Stukel et al., 2017 ~~and~~ & 2018; Boyd et al., 2019; Martin et al.,

2020). Many studies focus on the subduction of mode waters driven by large-scale circulation, and the seasonal cycle of the mixed layer dynamics (Williams, 2001; Qu et al., 2002; Qiu et al., 2007; Koch-Larrouy et al., 2010; Kawakami et al., 2015; Nie et al., 2016). But recent advances have highlighted the importance of small-scale (1-100 km) dynamical processes on vertical transport and biogeochemistry in the upper ocean, driven by mesoscale eddies and sub-mesoscale processes (Lévy et al., 2001; Xu et al., 2014; Omand et al., 2015; McGillicuddy, 2016; Llort et al., 2018; Resplandy et al., 2019). Ocean general circulation models typically resolve the large-scale subduction of mode waters (Koch-Larrouy et al., 2010) but cannot accurately capture small-scale, short-term subduction processes because of their episodic characteristics (Xu et al., 2014; Llort et al., 2018).
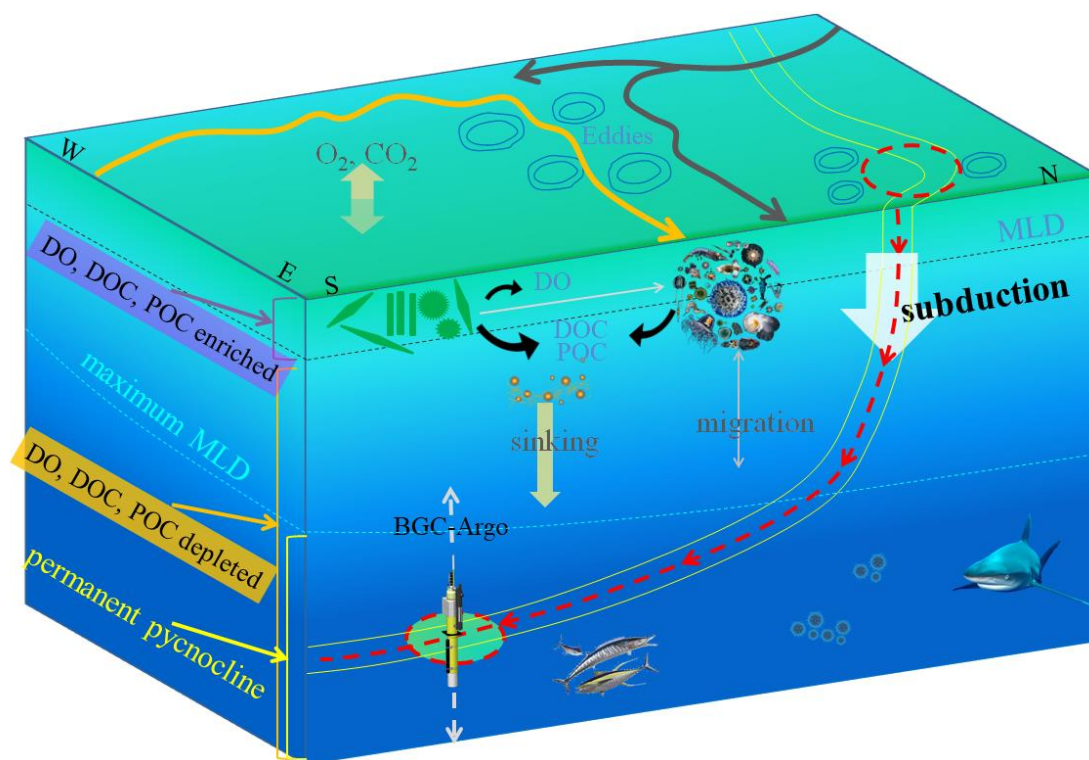
Fig. 1 An illustration of the Kuroshio and Oyashio extension region depicting the different modes of carbon export below the maximum annual mixed layer depth; the biologcial gravitational pump (sinking export, zooplankton migration) and subduction in the region of the Kuroshio and its extension (yellow line) and Oyashio and its extension (grey line). The subducted surface waters, apparently driven by mesoscale eddy processes, travel along isopycnal surfaces transporting water containing high dissolved oxygen (DO), dissolved organic carbon (DOC) and particulate organic carbon (POC) into the mesopelagic zone (low DO, DOC, and POC). The green layer represents the euphotic zone, and the blue layer below is the mesopelagic zone.

Subduction associated with mesoscale and sub-mesoscale dynamics has been observed at higher latitudes in the North Atlantic (Omand et al., 2015) and Southern Oceans (Llort et al., 2018), and similar processes are shown to occur in Kuroshio Extension

(KE) region in the western subtropical Pacific. Shipboard sampling techniques have been used there to identify small water parcels within the main thermocline having low potential vorticity, elevated dissolved oxygen (DO), and anomalous salinity; signals indicative of small-scale subduction (Yasuda et al., 1996; Okuda et al., 2001; Oka et al., 2009). Analogous phenomena have been observed in mooring data from the region (Nagano et al., 2016; Inoue et al., 2016a; Kouketsu et al., 2016; Zhu et al., 2021), and more focused sampling of anticyclonic eddies with Argo floats (Zhang et al., 2015; Inoue et al., 2016b) and SeaGliders (Hosoda et al., 2021) confirm the existence of discrete subsurface water mass exchanges. These episodic features will contribute to both ventilation of the mesopelagic zone as well as export of dissolved inorganic and organic carbon from surface waters (i.e., the solubility pump (Sarmiento & Gruber, 2006), but their frequency, spatial extent and lifetimes remain unknown (Hosoda et al., 2021).

Eddy-associated processes that generate vertical transport of productive and detrital planktonic biomass into the mesopelagic zone affect not only carbon export but also carbon sequestration time scales (i.e., time that carbon remains within the ocean interior). In general, sequestration time scales are proportional to the depth of injection but the more important factor is whether these injections extend below the annual maximum mixed layer depth (MLD), or permanent pycnocline, which hinders its return to the atmosphere (Boyd et al., 2019). Although eddy-subduction has the potential to contribute significantly to global carbon export, evidence of the subsurface fate of injected carbon has been indirect and patchy (Estapa et al., 2019), highlighting the challenge of detecting and quantifying carbon export associated with mesoscale and sub-mesoscale processes.

The uncertainty about the contribution of eddy subduction to carbon and oxygen transport into the mesopelagic and deeper ocean interior has ramifications for both biogeochemical and ecological processes (Fig. 1). The transport of freshly produced particulate and dissolved organic carbon, along with oxygen, from surface waters to the mesopelagic zone is critical for balancing upper ocean carbon budgets (Emerson, 2014) and supporting the nutritional demands of mesopelagic organisms (Dall'Olmo et al., 2016). The knowledge gap in these episodic processes is particularly evident in the mid-latitude western North Pacific, where mesoscale eddies, recirculation gyres, fronts, and jets are amplified under the influence of the Kuroshio and Oyashio currents and their extensions (Nishikawa et al., 2010). Shoaling of the maximum annual MLD in this region relative to higher latitudes (Cronin et al., 2013; Palevsky & Doney, 2018) has the potential to increase carbon sequestration efficiency and oxygenation of the deep mesopelagic zone (Bushinsky & Emerson, 2018).

Here we investigate small-scale subduction events in the western North Pacific region over the past decade (2008-2019). These events were identified with a new algorithm utilizing anomalies of apparent oxygen utilization (AOU; a proxy for dissolved and particulate organic matter degradation) and potential spicity (π; a characteristic water mass marker) obtained from multiple biogeochemical Argo (BGC-Argo) datasets

(Claustre et al., 2020; Chai et al., 2020). These findings show the spatial and temporal distributions of subduction patches reflecting episodic injection processes that contribute to the missing fraction of carbon and oxygen export into the deep twilight zone (Emerson, 2014; Martin et al., 2020), but also have the potential to become increasingly significant under future climate scenarios.

2. Data and Methods

2.1 Data

After the standard data quality control, 7,120 profiles from 43 BGC-Argo floats in the western North Pacific (20-50°N, 120-180°E) between 2008 and 2019 were selected (Fig. 2). All of these profiles contained measurements of temperature, salinity, pressure, and dissolved oxygen (DO, μmol/kg). The upper 1000db of the ocean was sampled in each profile and the typical profiling interval was between 5-10 days, with the floats parking at 1000db depth in between. The typical vertical sampling frequency was every 5db, 10db, and 50db for depth intervals of 0-100db, 100-500db, and 500-1000db, respectively. Some floats were set with daily profiling and higher vertical frequency (e.g., every 2db) for specific purposes.
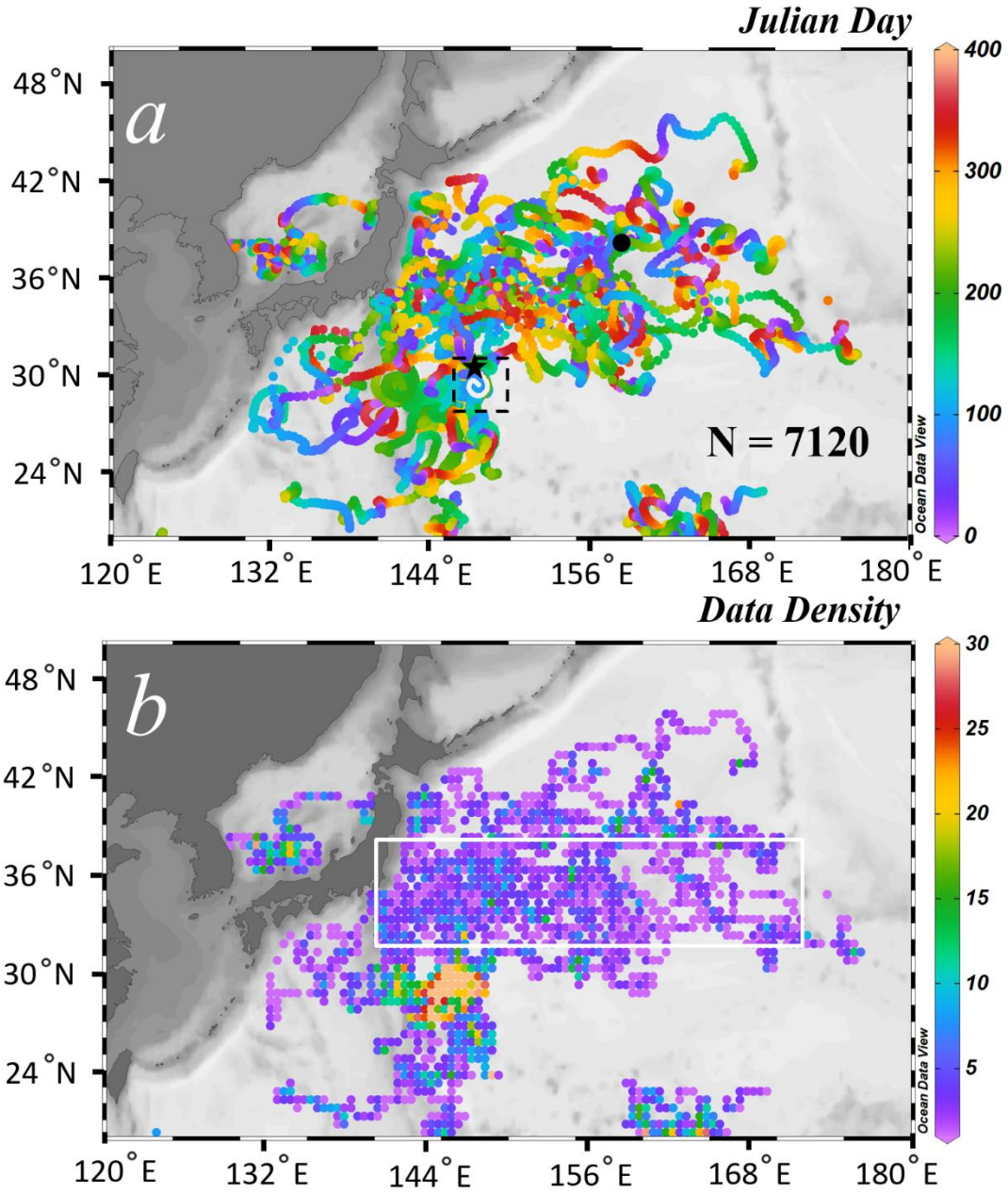
Fig. 2 Horizontal distribution of the QCed BGC-Argo data profiles between 2008 and 2019 in the western North Pacific. The argo profiling tracks are color coded by Julian day (a) and data density (number of available profiles) for each grid ($0.5^{\circ} \times 0.5^{\circ}$) (b). The location of Station No. 234 from float MD5904034 is denoted by the black dot in (a) (see Fig. 3); the white line in the dashed box represents the trajectory of float MR2901556 between July 28th and August 18th in 2014, and the black star indicates the beginning of the float trajectory during this period (see Fig. 4). The white box in (b) denotes the region with strong energetic ocean processes.

All BGC-Argo variables were vertically smoothed with a 3-bin running average to remove sharp noises or spikes (Llort et al., 2018). Two key variables, apparent oxygen

utilization (AOU) and potential spicity (π), were derived from the direct measurements. Specifically, AOU is defined as the difference between saturated oxygen concentration (O_{sat}) and DO, and O_{sat} is estimated from temperature and salinity (Garcia & Gordon, 1992). AOU is a proxy for water mass age which reflects the microbial respiration of dissolved and particulate organic matter (Sarmiento & Gruber, 2006). Potential spicity referenced to the surface pressure is calculated from pressure, temperature and salinity following Huang et al. (2018). Sea water is a two-component system. Water mass anomaly is commonly analyzed in term of (potential) temperature and salinity anomaly, and isopycnal analysis is also widely used. By definition, temperature and salinity anomaly on an isopycnal surface is density compensated; thus, water mass anomaly on an isopycnal surface is commonly described in term of another thermodynamic variable, which is called spice, spiciness or spicity. Over the past decades, there have been different definitions of such a thermodynamic variable; however, a most desirable property of such a thermodynamic function is that it is orthogonal to the density. Recently, Huang et al. (2018) proposed a potential spicity function (π) by the least square method, which is practically orthogonal to the potential density, with the root-mean-square of angle deviation from orthogonality at the value of $0.0001°$. Therefore, combining density and spicity gives rise to an orthogonal coordinate system, it is the thermodynamic variable we used in this study, ~~and it~~which allows differentiating water masses with distinct thermohaline properties but similar density. In addition, potential density (σ) referenced to the surface pressure was derived from pressure, temperature and salinity based on the thermodynamic equation (TEOS-10 (McDougall & Barker, 2011)); and MLD was estimated based on a threshold (0.05 kg/m^3) of the difference in density from a near-surface value (i.e., at 10db) (Brainerd & Gregg, 1995). All these derived variables were calculated for each of the 7,120 profiles.

In addition to the BGC-Argo float data, satellite data of daily sea level anomalies (SLA) and daily geostrophic velocity anomalies (*u'* and *v'*) between 1993 and 2018 were also processed. The geostrophic velocity anomalies were used to calculate the eddy kinetic energy (EKE) as $\text{EKE} = \frac{1}{2}\sqrt{u'^2 + v'^2}$. These data were used to identify the spatial relationship between surface mesoscale circulation and the float profiles.

2.2 Methods

2.2.1 subduction detection

When a BGC-Argo float passes through a parcel of water injected from the mixed layer, it captures coherent anomalous features in AOU and π distinct from the surrounding waters (Fig. 1). These anomalies can be used to identify subduction patches that are indicators of subduction events occurring in the vicinity (Omand et al., 2015; Llort et al., 2018). Quantifying anomalies in AOU and π (denoted as Δ_{AOU} and Δ_{π}) requires defining the reference values of AOU and π at the mean state of the profile without subduction. Llort et al. (2018) used the 20-bin running averages of the profiles as the references, however, we found that this approach could dampen the subduction signal and thus miss subduction patches as well as misidentify other signals as subduction (see

173   Fig. S1). To avoid misreporting these anomalies, a revised detection method was
174   developed by trial and error, as shown in example profiles of AOU, π, DO and σ for
175   Station No. 234 of float MD5904034 (Fig. 3; see Fig. 2a for its sampling location). Two
176   subduction patches are visually apparent at ~230db and ~300db (yellow shades in Fig.
177   3a & 3b). The identification of the lower subduction patch at ~300db from the spicity
178   profile is briefly described below and is illustrated in Fig. 3c:

179   1.   Calculate the slopes (i.e., first-order derivative) for profiles of AOU and π
180   against depth;

181   2.   Locate the peaks in AOU and π profiles (e.g., the blue star in Fig. 3c) based on
182   their slopes. Specifically, if at one sampling point the slope changes from
183   positive to negative when moving downwards, it is called a negative peak and
184   vice versa. Only the negative/positive peaks in π associated with a negative peak
185   in AOU are considered, as only negative AOU anomalies indicate potential
186   water transport from the surface mixed layer (Llort et al., 2018);

187   3.   Locate the coherent peaks in both AOU and π, and mark their depths as the
188   targeted locations (represented by pressure, p) for potential subduction patches;

189   4.   Calculate the peak Δ_π at each targeted pressure. For the case of a negative
190   (positive) peak, identify the maximum (minimum) values of π within the depth
191   ranges of [p-Δp, p] and [p, p+Δp], respectively (green triangles in Fig. 3c), and
192   the depth interval Δp=100db is chosen, considering the general vertical scale
193   (i.e., a few tens of meters) of the eddy-induced subduction features (Zhang et
194   al., 2015; Hosoda et al., 2021); the reference profile is defined by the straight
195   line in between. The anomaly Δ_π (red bracket in Fig. 3c) is defined as the
196   difference between the reference profile and the original profile of π at pressure
197   p (green star in Fig. 3c);

198   5.   Calculate Δ_{AOU} using the same method, independent of Δ_π;

199   6.   The thresholds used to determine whether the signals meet the criteria of a
200   subduction patch or not were set to -10 μmol/kg for Δ_{AOU} and ±0.05 kg/m^3 for
201   Δ_π following Llort et al. (2018).

202
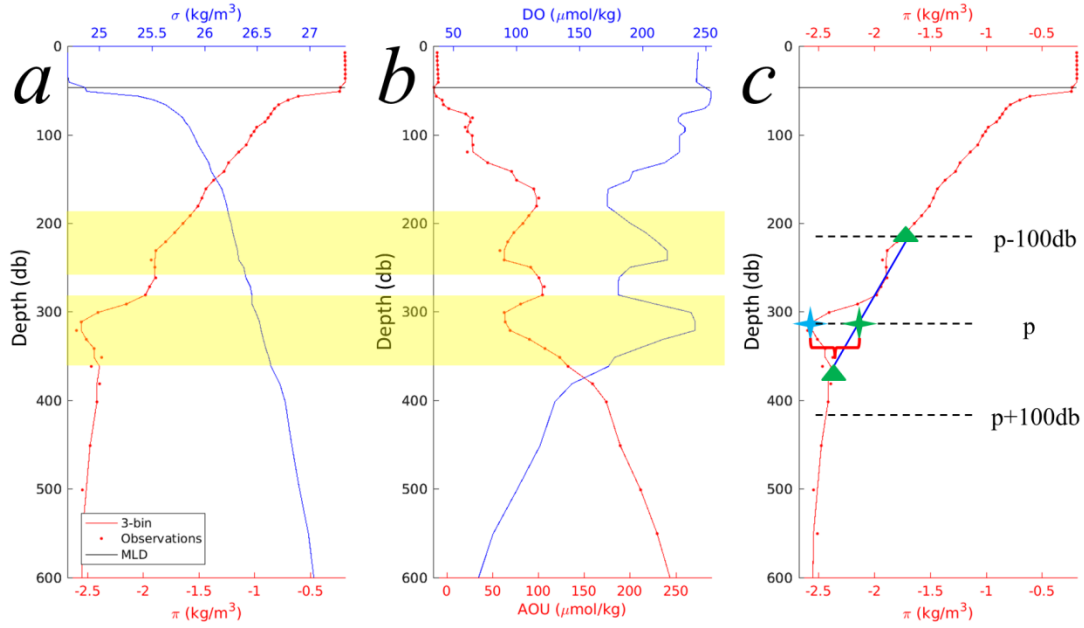
Fig. 3 Vertical property distributions of profile No. 234 (on June 24th 2016) of float MD5904034 (the black dot in Fig. 2a) demonstrate subduction patches observed by the BGC-Argo floats. (a) The profiles of potential density (σ, blue line) and potential spicity (π, red dotted line), (b) the profiles of DO (blue line) and AOU (red dotted line), and (c) same spicity profile as in (a), which is used to demenstrate the steps to detect subduction signals described in Methods. Note that the red dots in each panel represent the raw field observations, the overlaid red curves are the 3-bin running averages to remove sharp noises or spikes, and they are used to calculate the anomalies in AOU and π, and the black line represents the MLD. The yellow shades in (a) and (b) highlight the subduction features identified using the detection method in (c).

The refined algorithm presented here had improved performance for detecting subduction patches in these BGC-Argo profile data than that used in previous studies (Llort et al., 2018) (see Fig. S1). The main difference in our approach is in selecting the frame of reference for identifying AOU and π anomalies from irregular features in "typical" vertical profiles. ~~We speculate that our refinements here may reveal more episodic subduction patches in other datasets as well.~~

The sensitivity of the method to the interval of Δp (in step 4) was investigated by varying Δp between 70db and 130db (see Table S1). For Δp of 100±3db (i.e., 97db, 98db, 99db, 101db, 102db, and 103db), less than 7 ($\leq$ 2%) subduction patches were missed, and the resulted Δ_{AOU} and Δ_π show a RMSD of $\leq$ 3.8μmol/kg ($\leq$ 8.3%) and $\leq$ 0.03 kg/m3 ($\leq$ 9.2%). More details are provided in Text S1. The sensitivity analysis suggests the validity and robustness in the choice of Δp of 100db. After verifying that ~~this modified~~our approach better captured subduction indicators in a subset of BGC-Argo data from this region, the algorithm was applied to all profiles to identify the locations, depths, time and strengths (i.e., Δ_{AOU}, Δ_{DO} and Δ_π) of the subduction patches.

2.2.2 Quantification of ~~carbon and~~ oxygen export

For all the subduction patches identified using the method developed above, we obtain a first order estimate of ~~carbon and~~ oxygen export based on the ~~AOU anomalies (ΔAOU) and~~ DO anomalies (ΔDO) with the assumptions that: 1) the surface processes initiating these subduction events generated similar levels of DO (i.e., surface phytoplankton production ~~(i.e., organic carbon)~~), and 2) the water parcels containing this ~~organic carbon and~~ DO are subducted into the ocean's interior.

We ~~begin by estimating~~ estimated the average ~~carbon and~~ oxygen inventories within the water column based on the BGC-Argo profiles. We calculated ~~AOU and~~ DO inventories (per m^2) through these features in two ways: integration of the anomaly above the estimated baseline (Eq~~s~~. 1 ~~& 2~~) and by using the anomaly peak height (Eq~~s~~. ~~2~~3 ~~& 4~~) (see Fig. 3c). ~~The integrated AOU inventory was converted to carbon using a Carbon:Oxygen (C:O) remineralization ratio of 117:170 (Anderson and Sarmiento, 1994; Feely et al., 2004).~~

The equation~~s~~ for the integrated estimates for each profile ~~are~~is:

~~Carbon Inventory$_{IA}$ (g C/m^2) = C:O × $\sum_{z=p1}^{z=p2} \Delta AOU_z$~~ (Eq. 1)

Oxygen Inventory$_{IA}$ (g O$_2$/m^2) = $\sum_{z=p1}^{z=p2} \Delta DO_Z$ (Eq. ~~2~~1)

where ~~ΔAOU$_z$ and~~ ΔDO$_z$ ~~are~~ is the ~~AOU and~~ DO ~~anomalies~~ anomaly at depth z within the water column of the subduction patch, and the integrated areas (IA) of ~~AOU and~~ DO anomalies are converted from µmol kg^{-1} to mg m^{-2} based on seawater density.

The inventor~~ies~~y calculated using peak height (PH) approach ~~are~~is:

~~Carbon Inventory$_{PH}$ (g C/m^2) = C:O × Δ$_{AOU\_peak}$ × H~~ (Eq. 3)

Oxygen Inventory$_{\_PH}$ (g O$_2$/m^2) = Δ$_{DO\_peak}$ × H (Eq. ~~4~~2)

where H is the thickness (i.e., vertical height between the green triangles in Fig. 3c~~vertical range from depth p1 to p2~~, in unit of m) of the subduction patch and the ~~Δ$_{AOU\_peak}$ and~~ Δ$_{DO\_peak}$ ~~are~~ is the maximum anomalous value~~s~~ of ~~AOU and~~ DO converted to mg m^{-2} as above. The oxygen inventory using the peak height method represents the maximum potential of anomalous DO inventory within the subduction patch.

~~Converting these concentrations to carbon and oxygen export fluxes requires some knowledge of subduction rates, which can vary exponentially from surface (~100 m/day) to deep ocean (< 1 m/day). Rather than arbitrarily choosing a value in this range, we take a more conservative approach by considering that it is reasonable to expect that the subducted waters are renewed and dissipated on an annual scale. In other words, the individual subduction processes have at most a 1-year lifetime, and therefore we average the carbon and oxygen exports over 365 days (Eqs. 5-6).~~

264   ~~Carbon export (g C m^{-2} d^{-1}) = Carbon inventory / 365~~   ~~(Eq. 5)~~

265   ~~Oxygen export (g O$_2$ m^{-2} d^{-1}) = Oxygen inventory / 365~~   ~~(Eq. 6)~~

266   ~~using the inventories derived from Eqs. 1–4.~~

267   **7.3. Results and Discussion**

268   **3.1 Case study: Detecting subduction in BGC-Argo datasets**

269   Subduction associated with eddy pumping is a recognized important contributor to the
270   transfer of carbon and other materials from the surface euphotic layer to the ocean
271   interior (McGillicuddy, 2016; Bord et al., 2019), but investigating the spatial
272   distributions, physical dynamics, and biogeochemical consequences of these episodic
273   small-scale processes is difficult. The BGC-Argo program provides an exceptional data
274   resource for this purpose (Claustre et al., 2020; Chai et al., 2020), but detecting
275   subduction signals where differences among water masses are small is challenging.

276   Subduction below the seasonal and permanent pycnoclines can be identified in vertical
277   profiles by anomaly matrices of temperature, salinity, and dissolved oxygen (DO).
278   Examples of these events are illustrated in time-series from the BGC-Argo profiling
279   float (MR2901556), positioned on the southern perimeter of the Kuroshio Extension
280   region between July 28th and Aug. 18th 2014 (Fig. 4). Here, intermittent patches of
281   elevated spicity (π), lower AOU, and greater dissolved oxygen are visible in the upper
282   600 db (Boxes 1-3, Fig. 4). Potential spicity (π), a parameter dependent on pressure,
283   temperature and salinity (Huang et al., 2018), is a sensitive indicator of water mass
284   differences. AOU is the difference between the measured dissolved oxygen
285   concentration and its equilibrium saturation concentration in water with the same
286   physical and chemical properties. It reflects the degree of progressive microbial
287   decomposition of organic matter since the water was last at the surface in contact with
288   the atmosphere (Garcia & Gordon, 1992; Sarmiento & Gruber, 2006). Despite this
289   oxygen consumption, these injected waters retain excess net oxygen concentrations
290   relative to the surrounding mesopelagic zone (Fig. 4d).

291
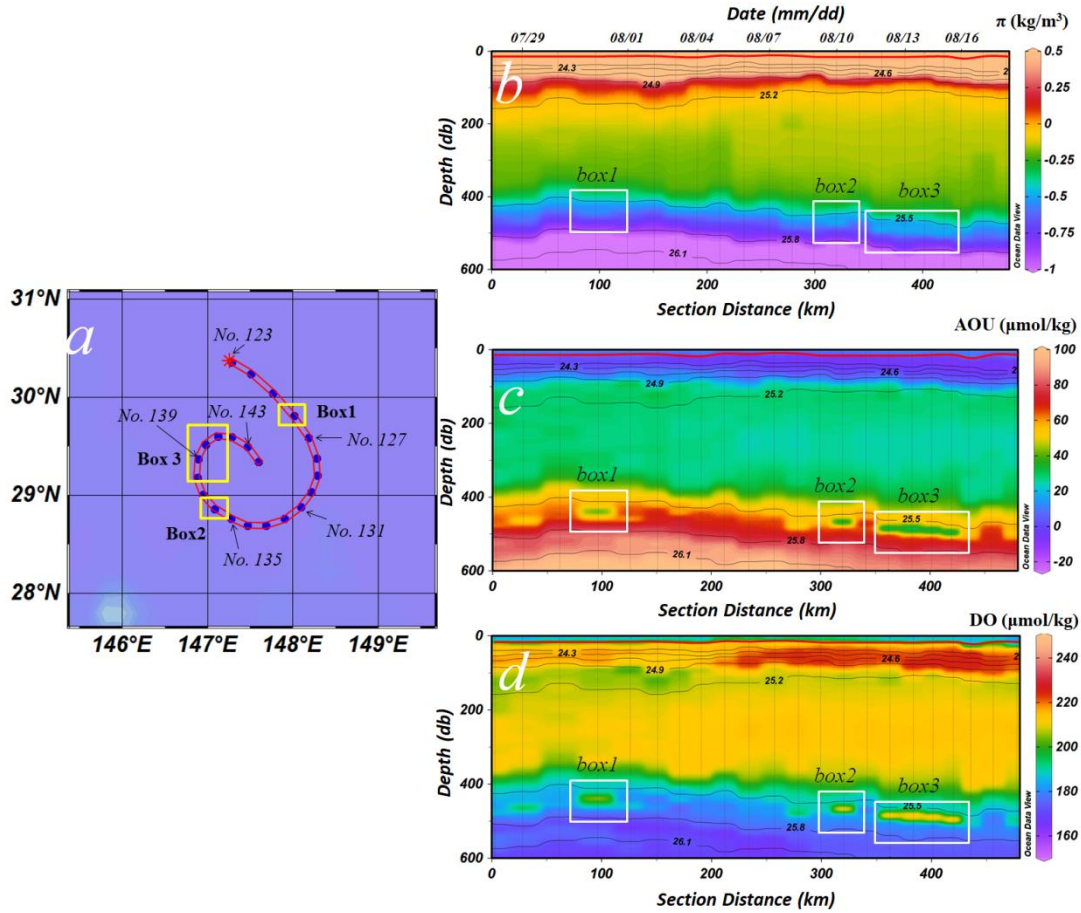
Fig. 4 Trajectory of float MR2901556 between July 28th 2014 (Station No. 123) and
August 18th, 2014 (Station No. 144) and its time series of π (b) AOU (c) and DO (d).
Vertical lines in (b), (c) and (d) represent the Bio-Argo profiles, and the section distance
along the X-axis is the path distance from Station No. 123 (the red star in (a)). The three
boxes (box1, box2, and box3) in panels (b,c,d) outline the coherent anomalous features
in π, AOU and DO, which were identified as subduction patches following the detection
procedure in Section 2.2.1. The red lines in panels (b,c,d) indicate the MLD, and the
horizontal black lines are the isopycnals. Anomalies of magnitude less than -10 μmol/kg
for Δ_{AOU} and ±0.05 kg/m^3 for Δ_{π} (e.g., at section distances of ~25km, 125km, 175km,
275km and 475km) were below our conservative thresholds for identifying intrusions
(-10 μmol/kg for Δ_{AOU} and ±0.05 kg/m^3 for Δ_{π}).

Llort et al. (2018) successfully identified eddy subduction in BGC-Argo data from the
Southern Ocean using anomalies in spiciness (Flament, 2002; Huang, 2011; McDougall
& Krzysik, 2015), a parameter derived from a different function of pressure,
temperature, and salinity than potential spicity (Huang et al., 2018). However, we found
that spiciness frequently missed signs of subduction while misidentifying other signals
as subduction, and the 20-bin method used by Llort et al. (2018) significantly dampened
the subduction signals in our data. Potential spicity (π) (Huang et al., 2018), on the other
hand, greatly improves the ability to distinguish among similar water masses due to its
orthogonal coordination with density; a feature that spiciness lacks. This added

sensitivity revealed reliable ~~substantially more~~ signals of subduction in these BGC-Argo data ~~than had been previously recognized~~. The ~~modified~~ algorithm based on peak detection here shows better capabilities in capturing and quantifying the subduction signals (see Methods, Fig. S1).

For the same subduction event, continuous subduction patches are expected to be identified from the Argo profiles. The ~~ephemeral nature of the~~ discrete anomalous π and AOU signals, highlighted in boxes 1-3 in the example time series (Fig. 4a, b, c, and d; July 31st, Aug 10th, and August 12th to 15th) indicates that they stemmed from distinct subduction events, opportunistically captured by this BGC-Argo float. The first two anomalies (July and early August) each appeared in only a single profile, perhaps indicating a limited spatial scale of these subduction events. In contrast, the mid-August anomaly persisted over 4 consecutive profiles~~,~~. We further examined the corresponding time series of temperature, salinity, and potential density, and found salinity also showed similar anomalous signal. As such, we suspect the consecutive subduction patches were most likely from~~suggesting~~ a more sustained, or a larger spatial subduction event.

3.2 Spatial and temporal distributions of subduction

We used our ~~modified~~ peak detection algorithm with the π and AOU data and applied it to all 7,120 BGC-Argo profiles (2008-2019) in the western North Pacific (Fig. 5). ~~The modified~~Our algorithm resolved 335 subduction patches, spread over an unexpectedly large area in the western North Pacific. Overall, subduction patches were identified in 288 profiles (4.0%) (some profiles have multiple patches at different depths), with approximately 83% of these being concentrated in the Kuroshio-Oyashio extension region (Fig. 5a). High ($\geq$~~>10~~6 cm) climatologic sea level anomalies (SLA) and the corresponding distribution of Eddy Kinetic Energy (EKE) are evidence of the strong energetic ocean processes in this region (Fig. 5a & 5b). By contrast, far fewer subduction patches were identified in the less energetic region to the south of 29°N despite a higher BGC Argo sampling density (Fig. 2b), consistent with eddy-related processes being important for driving these subduction events. Even so, the true frequency of these events across the entire region is certain to have been under-sampled given their small scales relative to the dispersed BGC-Argo float positions.
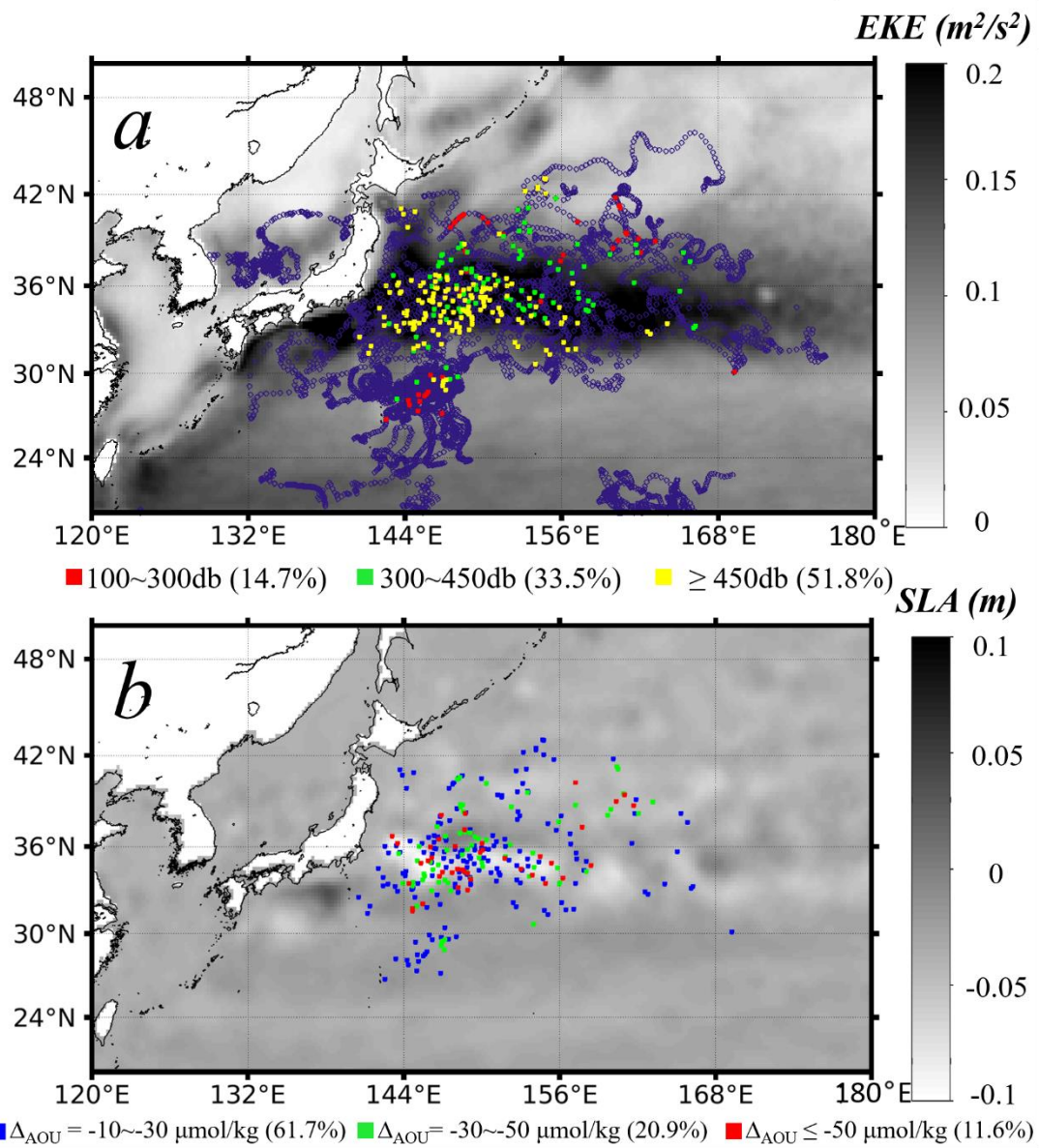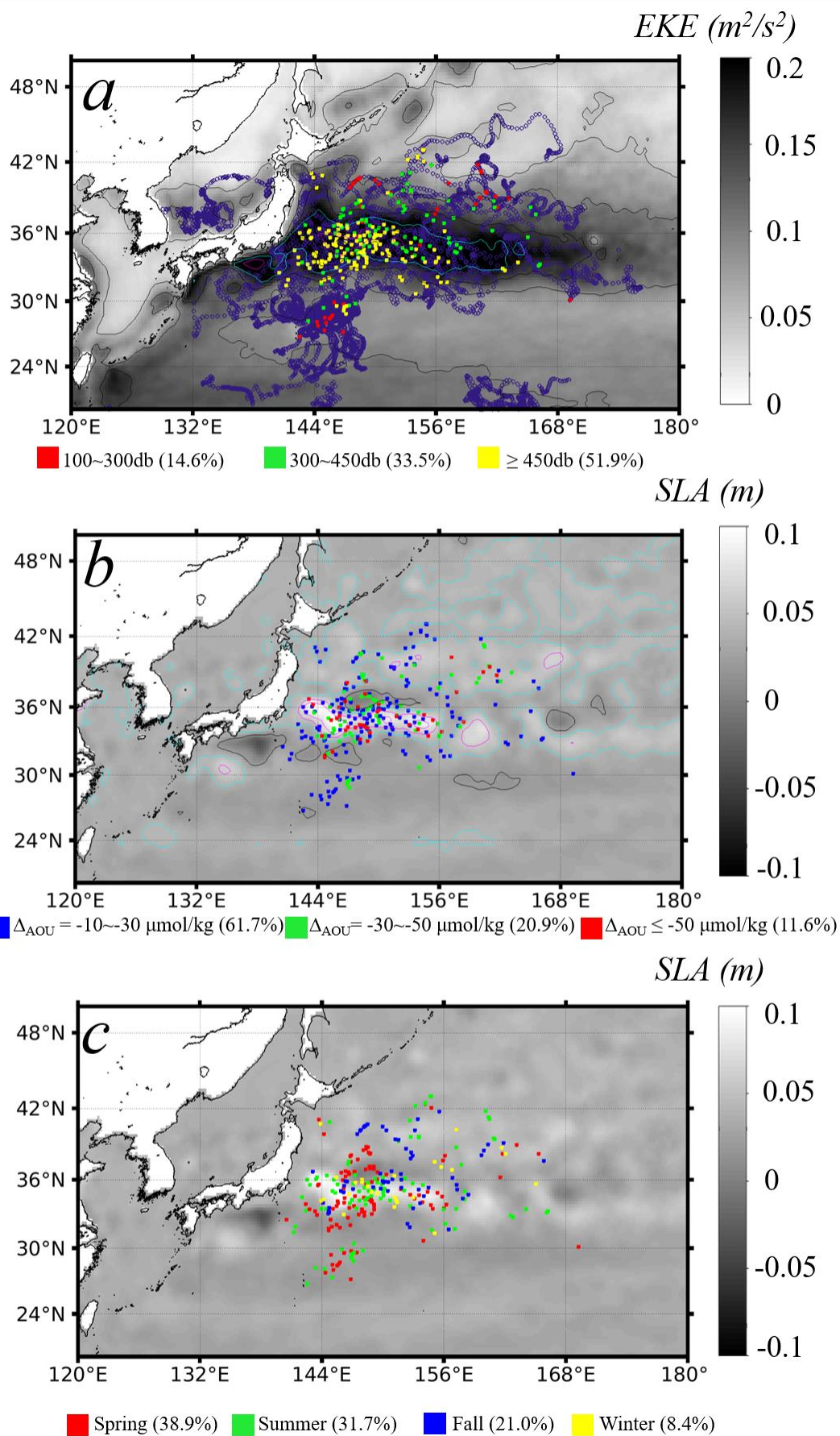
Fig. 5 Horizontal distribution of the BGC-Argo data profiles associated with subduction patches (a and b) between 2008 and 2019 in the western North Pacific. The profiles with detected subduction patches are color coded by different intervals of depths of the subduction patches (a), ~~and~~ AOU anomalies (b), and seasons (c), with percentages of detected patches in each interval annotated. ~~The grey-scale background maps in (a) and (b) are the annual mean EKE and SLA climatologies, and the~~ The purple background data in (a) represent all the analyzed profiles as shown in Fig. 2a. The grey-scale background map in (a) is the annual mean EKE climatology, with EKE contour lines of 0.3, 0.2, and 0.1 m^2/s^2 shown in magenta, cyan, and black, respectively, and the grey-scale background map in (b) is the annual mean SLA climatology, with SLA contour lines of $\geq$ 0.06, 0.04, and 0.02 m shown in magenta, cyan, and black, respectively. The seasons in (c) is divided with Spring of March-May, Summer of June-Auguest, Fall of September-November, and Winter of December-Febuary.

Discrete signals of subduction were detected throughout the mesopelagic depth range (~100-1000db), with the majority detected below 300db (green and yellow dots in Fig. 5a). The deepest penetrations ($\geq$450 db) occurred largely in areas experiencing the highest EKE while the shallowest (100-300 db) were largely restricted to areas with lower EKE (Fig. 5a). Based on 16 years' Argo float data (N = 1,226,177) in the global ocean, Feucher et al. (2019) found that the depth of permanent pycnocline differs between the subtropical (i.e., < 35° N) and subpolar (> 35° N) regions, with the depth of permanent pycnocline to be 300 m and 450 m in the subpolar and subtropical sections of the western North Pacific. Similarly, using the limited BGC-Argo dataset used in this study (Fig. 2), we also found comparably shallower annual maximum MLD in the subpolar section than that in the subtropical section (see Fig. S2). As a result, 56 (16.7%) and 104 (31.0%) subduction patches were found to be above and below the depth the permanent pycnocline (i.e., 450 m) in the subtropical section; and in the subpolar section, 34 (10.1%) and 141 (42.1%) and subduction patches were above and below the permanent pycnocline (i.e., 300 m). ~~Overall, r~~Roughly half (52%) of the detected subduction signals were ~~within or~~ below ~~the permanent pycnocline (~~450 db~~)~~ in this region of the western North Pacific ~~(Cronin et al., 2013; Palevsky & Doney, 2018; Feucher et al., 2019)~~, while 22% penetrated far deeper (up to 800 db; Table S2 in supplemental materials).

There was a distinct seasonality in subduction, with most (~70%) signals being observed between March (the maximum) and August (Figs. 6 & S2). Although only 8.3% of the total profiles were obtained in March, they accounted for 17.3% of all observed subduction patches (Fig. S3~~2~~a), correspondingly, the monthly subduction detection rate (i.e., the number of profiles with identified subduction patches divided by the total number of profiles available) was the highest in March, at ~ 10% (Fig. S4). In a pioneering work, Stommel (1979) argued that a demon working in the ocean by selecting the later winter (typically for later March in the North Hemisphere) water mass properties and injecting them into the subsurface ocean. This mechanism is now called the Stommel Demon in dynamical oceanography (Huang, 2010). The high detection rate of episodic subduction patches in March was consistent with observations

of large-scale subduction in this region during late winter, because mesoscale and sub-mesoscale eddy activities are prevalent when large-scale subduction occurs (Qu et al., 2002; Qiu et al., 2007; Nishikawa et al., 2010; Liu & Huang, 2012; Zhang et al., 2014; Xu et al., 2014). The March to August time frame also coincides with the onset and establishment of warming-induced shoaling of the mixed layer depth, when winter-subducted waters are less likely to be re-entrained into surface waters by winds (Dall'Olmo et al., 2016; Palevsky & Doney, 2018). Indeed, based on all the BGC-Argo dataset in Fig. 2, we found that the monthly MLD reached maximum in February and March, and then decreased until August. It should be noted that, despite the number of subduction patches identified in the time frame of April-August was slightly larger than those in September-December (Fig. S3a), the detection rates did not vary much between these time frames (Fig. S4). In contrast, comparatively few (3.0%) of the subduction patches were detected in January and February, in which time the detection rates were also low (<2%, Fig. S4). Although specific timelines between the observed subduction patches and their formation could not be determined, it is reasonable to anticipate that more energetic winds and the accumulated strong heat loss during mid-winter contributed to the peak in subduction signatures observed in March. However, there were no spatial patterns of the subduction patches detected in each season (Fig. 5c). The current BGC-Argo profiling asset is not sufficient to study how those subduction patches change on interannual scales.

408
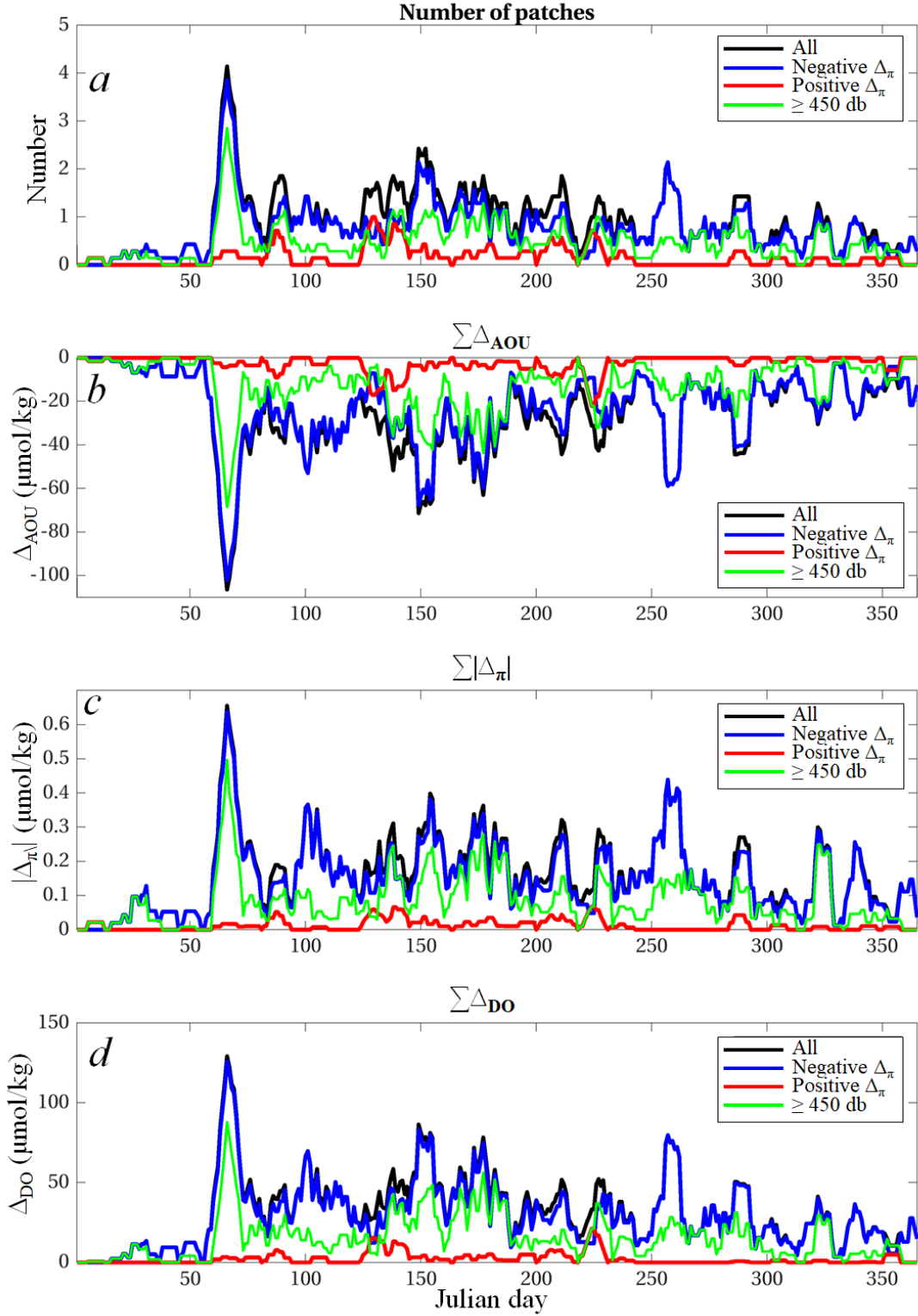
Fig. 6 Temporal distribution of the number of patches (a), integrated AOU anomaly (b), integrated π anomaly (c), and integrated DO anomaly (d), by Julian day based on 7-point smoothing. Spicity in subducted patches can be lower or higher than the surrounding waters, resulting in negative Δπ (red lines) or positive Δπ (blue lines) anomalies, respectively (see text in Section 3.4).

414 The Kuroshio-Oyashio extension zone lies between the subtropical and subpolar gyres
415 in the North Pacific, and it is a recognized hot-spot for water mass exchange via eddy
416 transport (Yasuda et al., 1996; Talley, 1997; Joyce et al., 2001; Zhang et al., 2014; Xu
417 et al., 2016) and substantial ocean-to-atmosphere heat flux (Jing et al., 2020). It is not
418 surprising then that the majority of subduction signals were observed in this region in
419 spite of less float coverage (Fig. 5). Large-scale circulation and seasonal variability in
420 the mixed layer depth here typically result in late winter subduction of subtropical mode
421 waters (Qiu et al., 2007; Oka et al., 2009; Oka & Qiu, 2012; Xu et al., 2014 & 2016),
422 and sharp horizontal density gradients can enhance strong vertical exchanges (Marshall
423 et al., 1993; Hurlburt et al., 1996; Liu et al., 2012; Ma et al., 2017). Rapid heat loss to
424 the winter-time cool, dry continental air masses flowing across the Kuroshio-Oyashio
425 extension erodes the seasonal thermocline to its maximum depth in February-March
426 (Cronin et al., 2013); the latter portion in which the subduction patches were most
427 frequently observed (Fig. 6).

428 Ascertaining the frequency and spatial extent of these lower-latitude episodic events
429 will be important for establishing their overall contribution to the transport of surface
430 waters into the mesopelagic zone, but this goal is challenged by the presently limited
431 distribution of BGC-Argo floats. It may be possible to obtain a first order estimate of
432 their frequency by linking the subduction signals here to surface-expressed indicators
433 of mesoscale circulation processes. Moreover, our findings suggest that spicity should
434 be adopted more generally in probing BGC-Argo datasets to improve our understanding
435 of the spatial and temporal distribution of subduction processes.

436 ~~3.3 Carbon and oxygen injections into the twilight zone~~

437 **3.3 Properties of subduction patch**

438 Beyond being a water mass indicator, AOU is a proxy for cumulative net community
439 respiration and a sensitive indicator of carbon export in the upper mesopelagic zone
440 (Emerson et al., 2001; Pan et al., 2014; Catala et al., 2018; Bushinsky & Emerson, 2018).
441 This export comprises remineralized carbon as well as dissolved and slowly sinking
442 particulate organic matter carried by the subducting waters (Stukel et al., 2017)⁻. The
443 magnitude of AOU may be used as an indicator of the time since subduction, with the
444 first order assumption being that the larger scale processes initiating these subduction
445 events generated similar surface production. Values of Δ_{AOU} at the anomalous peak
446 depth ranged between -10 (the minimal threshold used) and -81 µmol/kg (Fig. 7a). This
447 proxy was highly variable over the space-time domain, similar to the variations in Δ_{π}
448 (Fig. 7b). In general, 61.7% of the subduction patches had Δ_{AOU} in the range of -30 to
449 -10 µmol/kg with the remainder having greater oxygen depletions (i.e., $\leq$ -30 µmol/kg)
450 (Figs. 5b). Water masses subducted below 450db (i.e., the permanent pycnocline) had
451 an average AOU anomaly of -25.7±15.3 µmol/kg.
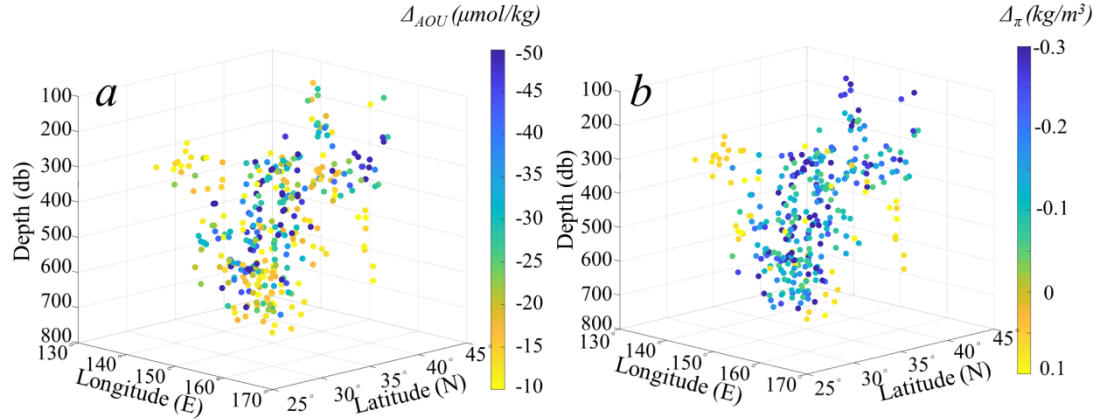
Fig. 7 Vertical spatial distribution of the detected subduction patches in the western North Pacific, color coded by the magnitudes of the subduction strengths in terms of AOU anomaly (a) and π anomaly (b), respectively.

There was no clear relationship between the depth of subduction and Δ_{AOU} ~~AOU~~ (Fig 7a), suggesting either surface production was substantially different when the sea-~~a~~-water parcels were subducted, or that these signatures stem from non-systematic differences in the time since subducted waters were last at the surface. The surface conditions (e.g., water temperature, primary productivity) really matter when the water parcels get subducted. On the other hand, it is noted in Fig. 7 that the depth positions of the subduction patches appear to somewhat extend from northeast to southwest and deeper along isopycnal surface as illustrated in Fig. 1. This phenomenon is clearly shown when averaging the depth of subduction patches both latitudinally and longitudinally (Fig. S5). Along the latitude, despite a few deep subduction patches identified at 42°-43° N (at around 550m), the mean depths of the subduction patches show a clear increasing pattern from latitude 37°-42° N to latitude of 32°-37° N, i.e., 300m vs. 500m. However, the depth positions tend to be shallower and shallower south of 32° N. Along the longitude, the depth positions generally appear to be deeper from east to west. As such, it is most likely that, the subduction occurred in the northern KE (37°-42° N) could traveled southwestward from shallow to deep depth, and these waters could reach 32° N. The increasing depth positions of subduction patches from 26° N to 32° N tend to suggest the gradually downward movements of the subducted water masses carried by the general trend of the anticyclonic gyre scale circulation, yet a further investigation is needed.

In the subpolar region, for the subduction patches identified above and below the depth of permanent pycnocline (i.e., 300 m), respectively, the averaged Δ_{AOU} are -32.9 and -25.8 μmol/kg, averaged Δ_{DO} are 42.5 and 32.5 μmol/kg, averaged thicknesses (i.e., vertical extension of the subduction patch) are 127.5 and 126.6 m (Table 1). In the subtropical region, the depth of permanent pycnocline was deeper (i.e., 450 m), the subduction patches above and below this layer were associated with a mean Δ_{AOU} of -27.2 and -28.5 μmol/kg, mean Δ_{DO} of 31.2 and 36.4 μmol/kg, and mean thickness of 128.7 and 128.1 m (Table 1). In general, the vertical extension (i.e., thickness) of the

subduction patches identified in each layer and in each region did not vary much between 126.6 m and 128.7 m. The mean Δ_{AOU} and Δ_{DO} were stronger above the depth of permanent pycnocline than those below the depth of permanent pycnocline in the subpolar region, yet the opposite case shows for the subtropical region, where the mean Δ_{AOU} and Δ_{DO} were weaker above the depth of permanent pycnocline than those below the depth of permanent pycnocline. Interestingly, it is noted that the mean Δ_{AOU} and Δ_{DO} in the subtropical region below 450 m were also weaker than those in the subpolar region above 300 m, which further supports the potential northeast-to-southwest pathway of subducted waters shown in Fig. 7.

Table 1 Statistics of the subduction patches and the associated oxygen exports into the ocean's interior. See Section 2.2.2 for details on the calculation of DO inventory. Note that these statistics are based on the subduction patches identified, without considering their episodic characteristics and spatial and temporal inhomogeinity.

Region	Layer	Number of patches	Mean ΔAOU (µmol/kg)	Mean ΔDO (µmol/kg)	Mean thickness (m)	DO inventory$_{IA}$ (g O$_2$ /m^2)	DO inventory$_{PH}$ (g O$_2$ /m^2)
Subtropical	< 450 m	56	-27.2±17.7	31.2±20.4	128.7±27.1	51.7±45.9	132.1±106.2
	≥ 450 m	104	-28.5±15.3	36.4±18.0	128.1±25.8	64.3±50.6	161.5±103.0
Subpolar	< 300 m	34	-32.9±15.5	42.5±17.7	127.5±35.0	92.6±59.7	197.5±115.3
	≥ 300 m	141	-25.8±15.9	32.5±20.9	126.6±23.2	61.2±53.1	142.1±108.1
Whole area	< 450 m	161	-29.7±16.7	36.7±19.7	126.8±26.8	68.5±52.8	160.5±108.0
	≥ 450 m	174	-25.6±15.2	32.5±19.8	128.2±25.1	59.4±52.5	144.3±108.0

Most subduction patches with strong AOU anomalies were observed between March and August (particularly March, see Fig. S3), after the seasonal mixed layer began to shoal, consistent with expected higher levels of phytoplankton production, which results in a greater degree of respiration in the subducted waters. More respiration means a great degree of oxygen consumption and thus a more negative offset from the surface-saturated concentrations before subduction. Only 0.6% of the total subduction patches had Δ_{AOU} of ≤ -30 µmol/kg in January and February (Fig. S2bS3b). It should be noted that Δ_{AOU} would also strongly depend on the water temperature (which determines the solubility of oxygen) when it gets subducted. The π anomalies show similar variation patterns with months (peaked in March), with stronger Δ_{π} coupled with stronger Δ_{AOU} (Fig. S2cS3c).

Eddy-associated pumping is one of several processes contributing to net global ocean carbon export (McGillicuddy, 2016; Boyd et al., 2019), but its importance is generally thought to be comparatively small because the relatively shallow penetration leads to shorter carbon sequestration times (Lévy et al., 2001; Karleskind et al., 2011a & 2011b; Omand et al., 2015; Nagai et al., 2015; Boyd et al., 2019). That is, much of the carbon "exported" to the upper mesopelagic zone over spring and summer is returned to the atmosphere by deep winter mixing. At higher latitudes, where eddy pumping has been most studied, subduction must extend up to > ~1000 m to reach below the permanent pycnocline (Palevsky & Doney, 2018; Boyd et al., 2019). However, the permanent

pycnocline in the western North Pacific is much shallower—on the order of ~400 db (Qiu & Huang, 1995; Feucher et al., 2019)—and most of the observed subduction signals here extended far below this depth (Table S2). Thus although the subduction depths shown here are similar to those observed at higher latitudes, they represent much longer carbon sequestration time scales than those previously associated with eddy pumping (Boyd et al., 2019).

Similar small-scale subduction processes carry both particulate and dissolved organic matter, and modeling suggests that this physical mechanism can be a major factor influencing export of carbon from surface mixed layers to the upper mesopelagic zone (McGillicuddy, 2016; Stukel et al., 2017 & 2018). In our case, the subduction patches contained on average negative AOU anomalies of -27.6±16.4 µmol/kg, with a maximum of -81 µmol/kg in March (Figs. 6 &7, Table 1); which are significantly stronger than that observed for eddy pumping processes in the Southern Ocean (Llort et al., 2018). This microbial oxygen consumption corresponds to remineralization of ~19-56 µmol C/kg. Carbon export rates within these subducting patches, based on the thickness of the subduction layer, the magnitude of AOU, and conservative estimates of advection rates, would be on the order of 85-218 mg C m^{-2} day^{-1} (Table 2); i.e., export rates similar in magnitude, but smaller in spatial scales, to that occurring in the North Atlantic spring bloom (Siegel et al., 2014). However, these values are likely an underestimate because only a portion of the organic carbon would have been degraded on these monthly time scales (Bushinsky & Emerson, 2018). Even so, the overall regional export associated with these events is difficult to estimate given that the subduction patches were only opportunistically captured by a comparatively wide separation of BGC-Argo profiles. The true frequency of these events is unknown.

The inferred injection dynamics observed here would partially offset the apparent imbalance between the biological gravitational pump and mesopelagic carbon budgets (Burd et al., 2010; Emerson, 2014) as well as the nutritional shortfalls for subsurface biota (Steinberg et al., 2008; Oka et al., 2009; Lacour et al., 2017). The intensity of these export events below the permanent pycnocline is remarkable, and they have not been adequately considered in biogeochemical models.

Table 1 Summary of the subduction patches associated with positive and negative π anomalies; red numbers indicating statistics of the sum and mean based on absolute values of π anomalies.

Table 2 Statistics of the subduction-injected carbon and oxygen exports and export rates into the ocean's interior. See Section 2.2.2 for details on the calculation. Note that these statistics are based on the subduction patches identified, without considering their episodic characteristics and spatial and temporal inhomogeinity.

Method	Carbon Inventory (g C/m²)	Oxygen Inventory (g O$_2$/m²)	Carbon export (mg C/m²/day)	Oxygen export (mg O$_2$/m²/day)
Integrated Area	31.3±25.9	63.8±52.8	85.8±71.1	174.6±144.6

Peak Height	79.8±58.1	152.1±108.1	218.6±159.1	416.6±296.2

556

3.4 Oxygen injections into the twilight zone

Global ocean inventories of oxygen have been decreasing, and current climate models predict this trend is likely to accelerate over the next century (Oschlies et al., 2018). However, these models suffer from considerable gaps in understanding, one of which is the absence of small-scale transport processes such as the events captured here (Oschlies et al., 2018). The average residual DO enrichment in the subduction patches, defined as the difference in DO concentrations within and adjacent to the subducted waters, was 34.5±19.8 μmol O_2/kg, with levels as high as ~88 μmol O_2/kg below 450 db during March (~~Table 1,~~ Figs. 6 & 7). These differences reflected ~20% higher oxygen concentrations than in the surrounding mesopelagic waters. Based on these residual excess oxygen concentrations ~~and very conservative estimates of advection rates~~, the oxygen ~~flux~~ inventory within these features ~~would~~ was estimated to be on the order of~~–~~ 64 to 152~~174-417~~ ~~m~~g O_2 m^{-2} ~~(Eqs. 1 & 2)day^{-1}~~. Specifically, the DO inventories below the permanent pycnocline in the subtropical and subpolar regions were on the order of 64.3-161.5 g O_2 m^{-2} and 61.2-142.1 g O_2 m^{-2}, respectively (Table ~~2~~1). These oxygen ~~fluxes are ~ 3-6 times greater than the estimated mesopelagic oxygen consumption rates in the highly productive Atlantic sector of the Southern Ocean (Dehairs et al., 1997), and thus~~ may represent a significant source of ventilation to our study region.

576

Co-injection of oxygen below the permanent pycnocline by eddy pumping has not been given close consideration in previous studies, largely because it is less relevant for high latitude, oxygen-rich waters. However, weak ocean ventilation in the tropical and subtropical mesopelagic zone is leading to declining oxygen concentrations (Karstensen et al., 2008; Oschlies et al., 2018; Robinson, 2019) and expansion of oxygen minimum zones in many regions of the oceans (Stramma et al., 2008; Breitburg et al., 2018). These episodic, dispersed subduction events likely represent a significant source of ventilation to help offset the de-oxygenation phenomenon, and to support the expected climate-driven effects of increasing temperature on the metabolic oxygen demand of mesopelagic organisms (Wohlers et al., 2009). Enriched oxygen supplies into the mesopelagic zone also will influence remineralization rates of sinking particulate organic carbon in the ocean's twilight zone (Buesseler et al., 2007; Steinberg et al., 2008) affecting carbon sequestration time scales. Current global-scale biogeochemical models ~~currently~~ are too coarse to capture the effect that these sub-mesoscale processes may have on mesoscale oxygen variability (Takano et al., 2018), or to account for this ~~added~~ additional oxygen supply. Overall, the intensity of these export events below the permanent pycnocline is remarkable, and they should be adequately considered in biogeochemical models.

Eddy associated pumping is also one of several processes contributing to net global ocean carbon export (McGillicuddy, 2016; Boyd et al., 2019), but its importance is generally thought to be comparatively small because the relatively shallow penetration leads to shorter carbon sequestration times (Lévy et al., 2001; Karleskind et al., 2011a & 2011b; Omand et al., 2015; Nagai et al., 2015; Boyd et al., 2019). That is, much of the carbon "exported" to the upper mesopelagic zone over spring and summer is returned to the atmosphere by deep winter mixing. At higher latitudes, where eddy pumping has been most studied, subduction must extend up to > ~1000 m to reach below the permanent pycnocline (Palevsky & Doney, 2018; Boyd et al., 2019). However, the permanent pycnocline in the western North Pacific is much shallower—on the order of ~3400-450 db (Qiu & Huang, 1995; Feucher et al., 2019)—and most of the observed subduction signals here extended far below this depth (Table S21 & S2). Thus although the subduction depths shown here are similar to those observed at higher latitudes, they represent much longer carbon sequestration time scales than those previously associated with eddy pumping (Boyd et al., 2019). As such, in addition to oxygen exports, the observed subduction patches seem to also transport large amounts of carbon into the ocean interior particularly below the permanent pycnocline. However, the lack of carbon measurements on the BGC-Argo floats used in this study impeded us to quantify the carbon inventory within the subduction patches.

Because the BGC-Argo profiler only captures snapshots of subduction events, it is impossible to quantify the vertical transporting rate, which is needed to quantify export fluxes, of subduction from the BGC-Argo float data alone. Alternatively, the lifetime of subduction patches could be used to infer subduction rates, yet due to the dynamics and episodic characteristics of eddy subduction, currently there is no estimates of how much time these water masses maintain differentiated properties in the mesopelagic zone, and there are numerous physical and biogeochemical processes influencing them. Similar small-scale subduction processes carry both particulate and dissolved organic matter, and modeling suggests that this physical mechanism can be a major factor influencing export of carbon from surface mixed layers to the upper mesopelagic zone (McGillicuddy, 2016; Stukel et al., 2017 & 2018). In our case, the subduction patches contained on average negative AOU anomalies of -27.6±16.4 µmol/kg, with a maximum of -81 µmol/kg in March (Figs. 6 &7, Table 1); which are significantly stronger than that observed for eddy pumping processes in the Southern Ocean (Llort et al., 2018). This microbial oxygen consumption corresponds to remineralization of ~19-56 µmol C/kg. Carbon export rates within these subducting patches, based on the thickness of the subduction layer, the magnitude of AOU, and conservative estimates of advection rates, would be on the order of 85-218 mg C m^{-2} day^{-1} (Table 2); i.e., export rates similar in magnitude, but smaller in spatial scales, to that occurring in the North Atlantic spring bloom (Siegel et al., 2014). However, these values are likely an underestimate because only a portion of the organic carbon would have been degraded on these monthly time scales (Bushinsky & Emerson, 2018). Even so, the overall regional export associated with these events is difficult to estimate given that the

646

3.54 Surface forcing of subduction

648 The AOU, DO and π anomalies were integrated within the study domain over the year
649 to assess the extent of subduction in the western North Pacific (Fig. 6, Table 12). π
650 anomalies were divided into negative or positive Δ_π—i.e., π being greater or less than
651 that in surrounding waters—which can suggest their modes of formation. Negative Δ_π
652 would correspond with the subduction of colder and less saline waters, such as along
653 the edges of cyclonic eddies, while positive Δ_π would be associated with the eddy
654 pumping of warmer core, anticyclonic eddies. The subduction patches were clearly
655 dominated by negative Δ_π, and more negative Δ_π corresponded with much larger Δ_{AOU}
656 and Δ_{DO} (Fig. 6, Table 2), suggesting they were associated with cyclonic, cold core,
657 upwelling-dominated eddies that have higher oxygen solubilities, nutrient flux to the
658 surface, and thus higher plankton production. Conversely, the association of lower
659 Δ_{AOU} and Δ_{DO} with positive Δ_π would align with the lower oxygen solubility, nutrient
660 flux and plankton production expected for warmer core, downwelling anticyclonic
661 eddies. Moreover, the majority of deep intrusions had negative Δ_π (Fig. 6, Table 2)
662 consistent with colder waters following deeper isoclines. In contrast, anticyclonic
663 eddies would push warm, lower oxygen and less biomass containing waters to
664 shallower depths. These findings suggest that tracking the activity of cyclonic eddies in
665 regions with shoaling permanent pycnoclines (Chelton et al., 2011; McGillicuddy, 2016)
666 may be particularly important for quantifying these deeper subduction processes.

Table 2 Summary of the subduction patches associated with positive and negative π
anomalies; bold numbers indicating statistics of the sum and mean based on absolute
values of π anomalies.

Statistics	Number of patches	Δ_{AOU} (µmol/kg)		Δ_{DO} (µmol/kg)		Δ_π (kg/m^3)	
		$\sum \Delta_{AOU}$	mean(Δ_{AOU})	$\sum \Delta_{DO}$	mean(Δ_{DO})	$\sum \Delta_\pi$	mean(Δ_π)
Total	335	-9248.43	-27.61	11560.79	34.51	**58.57**	**0.17**
$\Delta_\pi < 0$	279	-8303.75	-29.76	10743.84	38.51	-54.16	-0.19
$\Delta_\pi > 0$	56	-944.68	-16.87	816.95	14.59	4.41	0.08
Ratio ($\Delta_\pi < 0/\Delta_\pi > 0$)	4.98	8.79	1.76	13.15	2.64	**12.28**	**2.47**

670

The findings here indicate that eddy associated subduction is an important mechanism driving ~~carbon sequestration and~~ oxygen enrichment below the permanent pycnocline across the western subtropical Pacific region, particularly near the Kuroshio Extension (KE). Moreover, the abundance of these discrete, small-scale subduction events almost certainly is under-sampled in the BGC-Argo dataset. The frequency of this subduction is expected to vary as the KE oscillates between two dynamic states—quasi-stable and unstable—linked to the Pacific Decadal Oscillation (PDO) or North Pacific Gyre Oscillation (NPGO) (Di Lorenzo et al., 2008). When quasi-stable, the KE jet shifts north and generates less eddy activity than the unstable, highly meandering southward KE jet, which reduces eastward transport and sharply increases eddy kinetic energy (Qiu & Chen, 2010; Lin et al., 2014). Superimposed on these KE oscillations has been an increase in the ratio of cyclonic to anticyclonic eddies associated with a climate-driven intensification of tropical storms in the western Pacific and the multidecadal trend of acceleration in Kuroshio flow (Zhang et al., 2020), suggesting that the importance of eddy-associated subduction processes in this region has been increasing, and may continue to increase in the future. This linkage needs to be considered in designing future ocean observation programs and modeling of global biogeochemical cycles to adequately capture the damping effects that eddy associated subduction may exert on increasing atmospheric CO_2 and de-oxygenation in the tropical and subtropical ocean.

~~8.~~4. Conclusion

Biogeochemical measurements obtained from the BGC-Argo float data provide new insights into the small-scale vertical water mass exchange in the ocean. In particular, spicity and AOU are key parameters in capturing the episodic subduction events and their significance. Although these floats cannot capture the full pathways of subduction, they provide the first-hand data on locations, depths, time, and strengths of episodic subduction patches. Here we analyze float data in the western North Pacific and show significant subduction export of dissolved oxygen ~~and carbon~~ to the mesopelagic zone particularly below the permanent pycnocline; thus, the BGC-Argo data available over the global oceans can be used to extend the current study to other oceanic regions. Carbon measurements are needed to quantify the carbon export associated with the subduction patches. These two factors— ~~increased~~ carbon export and re-oxygenation— would help to offset the apparent budget imbalance between the biological gravitational pump and mesopelagic carbon demand, and support the increasing metabolic oxygen demand of mesopelagic organisms as ocean warming continues.

Acknowledgements

This work was supported by the National Key Research and Development Program of China (2016YFC1401601), the National Natural Science Foundation of China (NSFC) projects (~~41730536 and~~ 41906159, 42030708, and 41730536), the Scientific Research Fund of the Second Institute of Oceanography, MNR (14283), and the Marine S&T Fund of Shandong Province for Pilot National Laboratory for Marine Science and Technology (Qingdao) (2018SDKJ0206).

Author contributions

S. C. was responsible for data processing and drafting the manuscript, R. X. H. and H. X. took the lead in data analysis from the view of physical oceanography, M. L. W. and F. C. contributed to the biogeochemical analysis, and F. C. designed and coordinated the overall research project. All authors contributed to the ideas and writing of this manuscript.

Competing interests

The authors declare no competing financial or research interests.

Data availability

The BGC-Argo data used in this study were collected and made freely available by the International Argo Program and the national programs that contribute to it (http://www.argo.ucsd.edu, http://argo.jcommops.org), archived in the Argo Global Data Assembly Centre (http://doi.org/10.17882/42182), and quality-controlled and made available by the China Argo Real-time Data Center (http://www.argo.org.cn). The satellite SLA and geostrophic velocity data are from the Archiving, Validation and Interpretation of Satellite Data in Oceanography (AVISO) and can be downloaded from the Copernicus Marine Environment Monitoring Service (https://marine.copernicus.eu/).

References

Boyd, P.W., Claustre, H., Levy, M., Siegel, D.A. and Weber, T., 2019. Multi-faceted particle pumps drive carbon sequestration in the ocean. Nature, 568(7752), 327-335.

Brainerd, K. E., & Gregg, M. C., 1995. Surface mixed and mixing layer depths. Deep Sea Research Part I: Oceanographic Research Papers, 42(9), 1521-1543.

Breitburg, D., Levin, L. A., Oschlies, A., Grégoire, M., Chavez, F. P., Conley, D. J., ... & Jacinto, G. S., 2018. Declining oxygen in the global ocean and coastal waters. Science, 359(6371), eaam7240.

Buesseler, K. O., Lamborg, C. H., Boyd, P. W., Lam, P. J., Trull, T. W., Bidigare, R. R., ... & Honda, M., 2007. Revisiting Carbon Flux Through the Ocean's Twilight Zone. Science, 316(5824), 567-570.

~~Burd, A. B., Hansell, D. A., Steinberg, D. K., Anderson, T. R., Arístegui, J., Baltar, F., ... & Kadko, D. C., 2010. Assessing the apparent imbalance between geochemical and biochemical indicators of meso and bathypelagic biological activity: What the@ $#! is wrong with present calculations of carbon budgets?. Deep Sea Research Part II: Topical Studies in Oceanography, 57(16), 1557-1571.~~

Bushinsky, S. M., & Emerson, S. R., 2018. Biological and physical controls on the oxygen cycle in the Kuroshio Extension from an array of profiling floats. Deep Sea Research Part I: Oceanographic Research Papers, 141, 51-70.

Catala, T. S., Martinez-Perez, A. M., Nieto-Cid, M., Alvarez, M., Otero, J., Emelianov, M., Reche, I., Aristegui, J., & Alvarez-Salgado, X. A., ~~(2018)~~. Dissolved Organic Matter (DOM) in the open Mediterranean Sea. I. Basin-wide distribution and

drivers of chromophoric DOM. Progress in Oceanography, 165, 35-51. doi:10.1016/j.pocean.2018.05.002

Chai, F., Johnson, K. S., Claustre, H., Xing, X., Wang, Y., Boss, E., ... & Sutton, A., 2020. Monitoring ocean biogeochemistry with autonomous platforms. Nature Reviews Earth & Environment, 1, 315-326.

Chelton, D. B., Schlax, M. G., & Samelson, R. M., 2011. Global observations of nonlinear mesoscale eddies. Progress in oceanography, 91(2), 167-216.

Claustre, H., Johnson, K.S. and Takeshita, Y., 2020. Observing the Global Ocean with Biogeochemical-Argo. Annual review of marine science, 12, 11.1-11.26.

Cronin, M. F., Bond, N. A., Farrar, J. T., Ichikawa, H., Jayne, S. R., Kawai, Y., Konda, M., Qiu, B., Rainville, L., & Tomita, H., 2013. Formation and erosion of the seasonal thermocline in the Kuroshio Extension Recirculation Gyre. Deep-Sea Research Part II-Topical Studies in Oceanography, 85, 62-74. doi:10.1016/j.dsr2.2012.07.018

Dall'Olmo, G., Dingle, J., Polimene, L., Brewin, R.J. and Claustre, H., 2016. Substantial energy input to the mesopelagic ecosystem from the seasonal mixed-layer pump. Nature Geoscience, 9(11), 820-823.

Dehairs, F., Shopova, D., Ober, S., Veth, C. and Goeyens, L., 1997. Particulate barium stocks and oxygen consumption in the Southern Ocean mesopelagic water column during spring and early summer: relationship with export production. Deep-Sea Research Part II: Topical Studies in Oceanography, 44(1): 497–516.

Di Lorenzo, E., Schneider, N., Cobb, K. M., Franks, P. J. S., Chhak, K., Miller, A. J., ... & Powell, T. M., 2008. North Pacific Gyre Oscillation links ocean climate and ecosystem change. Geophysical Research Letters, 35(8).

Emerson, S., Mecking, S., & Abell, J., 2001. The biological pump in the subtropical North Pacific Ocean: Nutrient sources, Redfield ratios, and recent changes. Global biogeochemical cycles, 15(3), 535-554.

Emerson, S., 2014. Annual net community production and the biological carbon flux in the ocean. Global Biogeochemical Cycles, 28(1), 14-28.

Estapa, M. L., Feen, M. L., & Breves, E., 2019. Direct observations of biological carbon export from profiling floats in the subtropical North Atlantic. Global Biogeochemical Cycles, 33(3), 282-300.

Feucher, C., Maze, G., & Mercier, H., 2019. Subtropical mode water and permanent pycnocline properties in the world ocean. Journal of Geophysical Research: Oceans, 124(2), 1139-1154.

Flament, P., 2002. A state variable for characterizing water masses and their diffusive stability: spiciness. Progress in Oceanography, 54(1-4), 493-501.

Garcia, H.E. and Gordon, L.I., 1992. Oxygen solubility in seawater: Better fitting equations. Limnology and oceanography, 37(6), 1307-1312.

Hosoda, S., Inoue, R., Nonaka, M., Sasaki, H., Sasai, Y., & Hirano, M., (2021). Rapid water parcel transport across the Kuroshio Extension in the lower thermocline from dissolved oxygen measurements by Seaglider. Progress in Earth and Planetary Science, 8(1), 1-19.

Huang, R. X., 2010. Ocean Circulation, wind-driven and thermohaline processes, Cambridge Press, 810pp.

Huang, R. X., 2011. Defining the spicity. Journal of Marine Research, 69(4-5), 545-559.

Huang, R.X., Yu, L.-S. and Zhou, S.-Q., 2018. Potential spicity defined by the least square method, Journal of Geophysical Research, Ocean, 123, 7351-7365.

Hurlburt, H.E., Wallcraft, A.J., Schmitz Jr, W.J., Hogan, P.J. and Metzger, E.J., 1996. Dynamics of the Kuroshio/Oyashio current system using eddy-resolving models of the North Pacific Ocean. Journal of Geophysical Research: Oceans, 101(C1), 941-976.

Inoue, R., Honda, M. C., Fujiki, T., Matsumoto, K., Kouketsu, S., Suga, T., & Saino, T., 2016a. Western North Pacific integrated physical-biogeochemical ocean observation experiment (INBOX): Part 2. Biogeochemical responses to eddies and typhoons revealed from the S1 mooring and shipboard measurements. Journal of Marine Research, 74(2), 71-99.

Inoue, R., Suga, T., Kouketsu, S., Kita, T., Hosoda, S., Kobayashi, T., ... & Kawano, T., 2016b. Western north Pacific integrated physical-biogeochemical ocean observation experiment (INBOX): part 1. Specifications and chronology of the S1-INBOX floats. Journal of Marine Research, 74(2), 43-69.

Jing, Z., Wang, S., Wu, L., Chang, P., Zhang, Q., Sun, B., ... & Chen, Z., 2020. Maintenance of mid-latitude oceanic fronts by mesoscale eddies. Science advances, 6(31), eaba7880.

Joyce, T. M., Yasuda, I., Hiroe, Y., Komatsu, K., Kawasaki, K., & Bahr, F., 2001. Mixing in the meandering Kuroshio Extension and the formation of North Pacific Intermediate Water. Journal of Geophysical Research: Oceans, 106(C3), 4397-4404.

Karleskind, P., Lévy, M., & Mémery, L., 2011a. Subduction of carbon, nitrogen, and oxygen in the northeast Atlantic. Journal of Geophysical Research: Oceans, 116(C2).

Karleskind, P., Lévy, M., & Mémery, L., 2011b. Modifications of mode water properties by sub-mesoscales in a bio-physical model of the Northeast Atlantic. Ocean Modelling, 39(1-2), 47-60.

Karstensen, J., Stramma, L., & Visbeck, M., 2008. Oxygen minimum zones in the eastern tropical Atlantic and Pacific oceans. Progress in Oceanography, 77(4), 331-350.

Kawakami, Y., Sugimoto, S., and Suga, T., 2015. Inter-annual zonal shift of the formation region of the lighter variety of the north pacific central mode water. Journal of Oceanography, 72(2), 1-10.

Koch-Larrouy, A., Morrow, R., Penduff, T. and Juza, M., 2010. Origin and mechanism of Subantarctic Mode Water formation and transformation in the Southern Indian Ocean. Ocean Dynamics, 60(3), 563-583.

Kouketsu, S., Inoue, R., & Suga, T., 2016. Western North Pacific integrated physical-biogeochemical ocean observation experiment (INBOX): part 3. Mesoscale variability of dissolved oxygen concentrations observed by multiple floats during S1-INBOX. Journal of Marine Research, 74(2), 101-131.

Lacour, L., Ardyna, M., Stec, K. F., Claustre, H., Prieur, L., Poteau, A., et al., 2017. Unexpected winter phytoplankton blooms in the North Atlantic subpolar gyre. Nature Geoscience, 10(11), 836-839.

Lévy, M., Klein, P. and Treguier, A.M., 2001. Impact of sub-mesoscale physics on production and subduction of phytoplankton in an oligotrophic regime. Journal of Marine Research, 59(4), 535-565.

Lin, P., Chai, F., Xue, H., & Xiu, P., 2014. Modulation of decadal oscillation on surface chlorophyll in the Kuroshio Extension. Journal of Geophysical Research: Oceans, 119(1), 187-199.

Liu, L. L. and Huang, R.X., 2012. The global subduction/obduction rates: Their interannual and decadal variability. Journal of Climate, 25(4), 1096-1115.

Liu, Y., Dong, C., Guan, Y., Chen, D., McWilliams, J. and Nencioli, F., 2012. Eddy analysis in the subtropical zonal band of the North Pacific Ocean. Deep Sea Research Part I: Oceanographic Research Papers, 68, 54-67.

Llort, J., Langlais, C., Matear, R., Moreau, S., Lenton, A. and Strutton, P.G., 2018. Evaluating Southern Ocean carbon eddy-pump from biogeochemical-Argo floats. Journal of Geophysical Research: Oceans, 123(2), 971-984.

Ma, X., Chang, P., Saravanan, R., Montuoro, R., Nakamura, H., Wu, D., Lin, X. and Wu, L., 2017. Importance of resolving Kuroshio front and eddy influence in simulating the North Pacific storm track. Journal of Climate, 30(5), 1861-1880.

Marshall, J.C., Williams, R.G. and Nurser, A.G., 1993. Inferring the subduction rate and period over the North Atlantic. Journal of Physical Oceanography, 23(7), 1315-1329.

Martin, A., Boyd, P., Buesseler, K., Cetinic, I., Claustre, H., Giering, S., ... & Robinson, C., 2020. The oceans' twilight zone must be studied now, before it is too late. Nature, 580, 26-28.

McDougall, T., & Barker, P., 2011. Getting started with TEOS-10 and the Gibbs Seawater (GSW) oceanographic toolbox. SCOR/IAPSO, WG127, pp 28.

McDougall, T. J., & Krzysik, O. A., 2015. Spiciness. Journal of Marine Research, 73(5), 141-152.

McGillicuddy, D.J., 2016. Mechanisms of Physical-Biological-Biogeochemical Interaction at the Oceanic Mesoscale. Annual Review of Marine Science, 8, 125-159.

Nagai, T., Gruber, N., Frenzel, H., Lachkar, Z., McWilliams, J. C., & Plattner, G. K., 2015. Dominant role of eddies and filaments in the offshore transport of carbon and nutrients in the California Current System. Journal of Geophysical Research: Oceans, 120(8), 5318-5341.

Nagano, A., Suga, T., Kawai, Y., Wakita, M., Uehara, K., & Taniguchi, K., 2016. Ventilation revealed by the observation of dissolved oxygen concentration south of the Kuroshio Extension during 2012–2013. Journal of Oceanography, 72(6), 837-850.

Nie, X., Gao, S., Wang, F., & Qu, T., 2016. Subduction of north pacific tropical water and its equatorward pathways as shown by a simulated passive tracer. Journal of Geophysical Research: Oceans, 121.

884   Nishikawa, S., Tsujino, H., Sakamoto, K. and Nakano, H., 2010. Effects of mesoscale
885   eddies on subduction and distribution of subtropical mode water in an eddy-
886   resolving OGCM of the western North Pacific. Journal of Physical Oceanography,
887   40(8), 1748-1765.
888   Oka, E., Toyama, K. and Suga, T., 2009. Subduction of North Pacific central mode
889   water associated with subsurface mesoscale eddy. Geophysical Research Letters,
890   36(8), L08607.
891   Oka, E. and Qiu, B., 2012. Progress of North Pacific mode water research in the past
892   decade. Journal of oceanography, 68(1), 5-20.
893   Okuda, K., Yasuda, I., Hiroe, Y., & Shimizu, Y., 2001. Structure of subsurface intrusion
894   of the Oyashio water into the Kuroshio Extension and formation process of the
895   North Pacific Intermediate Water. Journal of oceanography, 57(2), 121-140.
896   Omand, M.M., D'Asaro, E.A., Lee, C.M., Perry, M.J., Briggs, N., Cetinić, I. and
897   Mahadevan, A., 2015. Eddy-driven subduction exports particulate organic carbon
898   from the spring bloom. Science, 348(6231), 222-225.
899   Oschlies, A., Brandt, P., Stramma, L., & Schmidtko, S., 2018. Drivers and mechanisms
900   of ocean deoxygenation. Nature Geoscience, 11(7), 467-473.
901   Palevsky, H. I., & Doney, S. C., 2018. How choice of depth horizon influences the
902   estimated spatial patterns and global magnitude of ocean carbon export flux.
903   Geophysical Research Letters, 45, 4171–4179. https://doi.org/10.1029/
904   2017GL076498
905   Pan, X., Achterberg, E. P., Sanders, R., Poulton, A. J., Oliver, K. I., & Robinson, C.,
906   2014. Dissolved organic carbon and apparent oxygen utilization in the Atlantic
907   Ocean. Deep Sea Research Part I: Oceanographic Research Papers, 85, 80-87.
908   Qiu, B., & Huang, R. X., 1995. Ventilation of the North Atlantic and North Pacific:
909   subduction versus obduction. Journal of Physical Oceanography, 25(10), 2374-
910   2390.
911   Qiu, B., Chen, S. and Hacker, P., 2007. Effect of mesoscale eddies on subtropical mode
912   water variability from the Kuroshio Extension System Study (KESS). Journal of
913   Physical Oceanography, 37(4), 982-1000.
914   Qiu, B., & Chen, S., 2010. Eddy-mean flow interaction in the decadally modulating
915   Kuroshio Extension system. Deep Sea Research Part II: Topical Studies in
916   Oceanography, 57(13-14), 1098-1110.
917   Qu, T., Xie, S.P., Mitsudera, H. and Ishida, A., 2002. Subduction of the North Pacific
918   mode waters in a global high-resolution GCM. Journal of physical oceanography,
919   32(3), 746-763.
920   Qu, T. and Chen, J., 2009. A North Pacific decadal variability in subduction rate.
921   Geophysical Research Letters, 36(22), L22602.
922   Resplandy, L., Lévy, M. and Mcgillicuddy, D.J., 2019. Effects of eddy-driven
923   subduction on ocean biological carbon pump. Global Biogeochemical Cycles, 33(8),
924   pp.1071-1084.
925   Robinson, C., 2019. Microbial respiration, the engine of ocean deoxygenation.
926   Frontiers in Marine Science, 5, 533.

Sabine, C.L., Feely, R.A., Gruber, N., Key, R.M., Lee, K., Bullister, J.L., Wanninkhof, R., Wong, C.S.L., Wallace, D.W., Tilbrook, B. and Millero, F.J., 2004. The oceanic sink for anthropogenic CO_2. Science, 305(5682), 367-371.

Sarmiento, J.L., & Gruber, N., 2006. Ocean biogeochemical dynamics. Princeton University Press.

~~Siegel, D. A., Buesseler, K. O., Doney, S. C., Sailley, S. F., Behrenfeld, M. J., & Boyd, P. W., 2014. Global assessment of ocean carbon export by combining satellite observations and foodssessment of Global Biogeochemical Cycles, 28(3), 181-196.~~Stommel, H. M., 1979. Determination of water mass properties of water pumped down from the Ekman layer to the geostrophic flow below. Proc. Natl. Acad. Sci. U.S.A., 76, 3051-3055.

Steinberg, D. K., Van Mooy, B. A., Buesseler, K. O., Boyd, P. W., Kobari, T., & Karl, D. M., 2008. Bacterial vs. zooplankton control of sinking particle flux in the ocean's twilight zone. Limnology and Oceanography, 53(4), 1327-1338.

Stramma, L., Johnson, G. C., Sprintall, J., & Mohrholz, V., 2008. Expanding oxygen-minimum zones in the tropical oceans. science, 320(5876), 655-658.

Stukel, M.R., Aluwihare, L.I., Barbeau, K.A., Chekalyuk, A.M., Goericke, R., Miller, A.J., Ohman, M.D., Ruacho, A., Song, H., Stephens, B.M. and Landry, M.R., 2017. Mesoscale ocean fronts enhance carbon export due to gravitational sinking and subduction. Proceedings of the National Academy of Sciences of the United States of America, 114(6), 1252-1257.

Stukel, M.R., Song, H., Goericke, R. and Miller, A.J., 2018. The role of subduction and gravitational sinking in particle export, carbon sequestration, and the remineralization length scale in the California Current Ecosystem. Limnology and Oceanography, 63(1), 363-383.

Takano, Y., Ito, T., & Deutsch, C., 2018. Projected centennial oxygen trends and their attribution to distinct ocean climate forcings. Global Biogeochemical Cycles, 32(9), 1329-1349.

Talley, L. D., 1997. North Pacific Intermediate Water transports in the mixed water region. Journal of physical oceanography, 27(8), 1795-1803.

Williams, R.G., 2001. Ocean Subduction, in: Encyclopedia of Ocean Sciences. Elsevier, pp. 1982–1993.

Wohlers, J., Engel, A., Zöllner, E., Breithaupt, P., Jürgens, K., Hoppe, H. G., ... & Riebesell, U., 2009. Changes in biogenic carbon flow in response to sea surface warming. Proceedings of the national academy of sciences, 106(17), 7067-7072.

Xu, L., Xie, S.P., McClean, J.L., Liu, Q. and Sasaki, H., 2014. Mesoscale eddy effects on the subduction of North Pacific mode waters. Journal of Geophysical Research: Oceans, 119(8), 4867-4886.

Xu, L., Li, P., Xie, S.P., Liu, Q., Liu, C. and Gao, W., 2016. Observing mesoscale eddy effects on mode-water subduction and transport in the North Pacific. Nature communications, 7, 10505.

Yasuda, I., Okuda, K., & Shimizu, Y., 1996. Distribution and modification of North Pacific Intermediate Water in the Kuroshio-Oyashio interfrontal zone. Journal of physical oceanography, 26(4), 448-465.

971   Zhang, Z., Wang, W., & Qiu, B., 2014. Oceanic mass transport by mesoscale eddies.
972   Science, 345(6194), 322-324.
973   Zhang, Z., Li, P., Xu, L., Li, C., Zhao, W., Tian, J., & Qu, T., (2015). Subthermocline
974   eddies observed by rapid-sampling Argo floats in the subtropical northwestern
975   Pacific Ocean in Spring 2014. Geophysical Research Letters, 42(15), 6438-6445.
976   Zhang, Y., Zhang, Z., Chen, D., Qiu, B., & Wang, W., 2020. Strengthening of the
977   Kuroshio current by intensifying tropical cyclones. Science, 368(6494), 988-993.
978   Zhu, R., Chen, Z., Zhang, Z., Yang, H., & Wu, L., 2021. Subthermocline eddies in the
979   Kuroshio Extension region observed by mooring arrays. Journal of Physical
980   Oceanography, 51(2), 439-455.